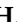



Article

Removal of Ni(II) Ions by Poly(Vinyl Alcohol)/Al₂O₃ Nanocomposite Film via Laser Ablation in Liquid

Fatemah H. Alkallas ¹, Hoda A. Ahmed ^{2,3}, Tahani A. Alrebdi ¹, Rami Adel Pashameah ⁴,
Salhah H. Alrefae ³, Emaan Alsubhe ⁵, Amira Ben Gouider Trabelsi ¹, Ayman M. Mostafa ^{6,7,*}
and Eman A. Mwafy ^{7,8}

- ¹ Department of Physics, College of Science, Princess Nourah bint Abdulrahman University, P.O. Box 84428, Riyadh 11671, Saudi Arabia; fhalkallas@pnu.edu.sa (F.H.A.); taalrebdi@pnu.edu.sa (T.A.A.); aatrabelsi@pnu.edu.sa (A.B.G.T.)
- ² Department of Chemistry, Faculty of Science, Cairo University, Cairo 12613, Egypt; ahoda@sci.cu.edu.eg
- ³ Chemistry Department, College of Sciences, Taibah University, Yanbu 30799, Saudi Arabia; srfay@taibahu.edu.sa
- ⁴ Department of Chemistry, Faculty of Applied Science, Umm Al-Qura University, Makkah 24230, Saudi Arabia; rapasha@uqu.edu.sa
- ⁵ Physics Department, Faculty of Science, Taibah University, Yanbu 30799, Saudi Arabia; esobhe@taibahu.edu.sa
- ⁶ Spectroscopy Department, Physics Division Institute, National Research Centre, 33 El Bohouth St. (Former El Tahrir st.), Dokki, Giza 12622, Egypt
- ⁷ Laser Technology Unit, Center of Excellent for Advanced Science, National Research Centre, 33 El Bohouth st. (Former El Tahrir St.), Dokki, Giza 12622, Egypt; emanmwafynrc@gmail.com
- ⁸ Physical Chemistry Department, Advanced Materials Technology and Mineral Resources Research Institute, National Research Centre, Giza 12622, Egypt
- * Correspondence: aymanmdarwish@gmail.com



Citation: Alkallas, F.H.; Ahmed, H.A.; Alrebdi, T.A.; Pashameah, R.A.; Alrefae, S.H.; Alsubhe, E.; Trabelsi, A.B.G.; Mostafa, A.M.; Mwafy, E.A. Removal of Ni(II) Ions by Poly(Vinyl Alcohol)/Al₂O₃ Nanocomposite Film via Laser Ablation in Liquid. *Membranes* **2022**, *12*, 660. <https://doi.org/10.3390/membranes12070660>

Academic Editor: Ahmed M. Khalil

Received: 5 June 2022

Accepted: 23 June 2022

Published: 27 June 2022

Publisher's Note: MDPI stays neutral with regard to jurisdictional claims in published maps and institutional affiliations.



Copyright: © 2022 by the authors. Licensee MDPI, Basel, Switzerland. This article is an open access article distributed under the terms and conditions of the Creative Commons Attribution (CC BY) license (<https://creativecommons.org/licenses/by/4.0/>).

Abstract: Al₂O₃-poly(vinyl alcohol) nanocomposite (Al₂O₃-PVA nanocomposite) was generated in a single step using an *eco*-friendly method based on the pulsed laser ablation approach immersed in PVA solution to be applicable for the removal of Ni(II) from aqueous solution, followed by making a physicochemical characterization by SEM, XRD, FT-IR, and EDX. After that, the effect of adsorption parameters, such as pH, contact time, initial concentration of Ni(II), and medium temperature, were investigated for removal Ni(II) ions. The results showed that the adsorption was increased when pH was 5.3, and the process was initially relatively quick, with maximum adsorption detected within 90 min of contact time with the endothermic sorption process. Moreover, the pseudo-second-order rate kinetics ($k_2 = 9.9 \times 10^{-4} \text{ g mg}^{-1} \text{ min}^{-1}$) exhibited greater agreement than that of the pseudo-first-order. For that, the Ni(II) was effectively collected by Al₂O₃-PVA nanocomposite prepared by an *eco*-friendly and simple method for the production of clean water to protect public health.

Keywords: PLAL; Al₂O₃; NPs; Nd:YAG; laser ablation; nanocomposite

1. Introduction

Nano adsorbent materials have sparked tremendous attention in recent years because of their large specific surface area, regular pore structure, and highly controlled surface characteristics. Almost the majority of the adsorbents that are created today to overcome the hazard of heavy metal ions and dyes depend on the engagement of the hazardous chemical compounds with the presence of functional groups on the adsorbents' surfaces [1–5]. As a result, the matrix's vast surface area and many adsorption sites are the most critical elements influencing the adsorbent's adsorption capacity. From hazardous chemical compounds, nickel waste is extremely dangerous to people, ecosystems, and animals. It has been found in a wide range of industrial wastes, including nickel–cadmium batteries, organic compounds, and insecticides [6–9]. The abundance of nickel ions in the water supply has been linked to a variety of major health issues, including carcinogenic agents.

As a result, removing nickel from wastewater and industrial pollutants is critical [10–13]. Several techniques have been employed to remove heavy metals from wastewater, including chemical precipitation, ion-exchange sorption, and solvent extraction. One of these methods, the adsorption method has been frequently employed because of its low cost and great efficacy [14–19].

Aluminum oxide nanostructured material (Al_2O_3) has been studied as a promising adsorbent for heavy metal ion elimination because of its large surface area. Moreover, in the water treatment field, it exhibits better catalytic activity in a variety of organic processes [20,21]. However, in the field of water treatment, powdered material is not suited for recycling. Furthermore, the separation of nanostructured materials from aqueous solutions is quite challenging, especially when the particle size is on the nano-scale. Researchers are currently concentrating on methods of employing nano-powder metal oxides to remove heavy metal ions [22–24]. One method is to incorporate nanoparticles into an organic substance, which could be represented by an optimum solution such as a polymer matrix structure. Adsorbent features such as surface area and functional groups on the adsorbent surface should be addressed for the adsorbent to eliminate heavy metal ions. The important qualities of the adsorbent, such as high mechanical and thermal stability and high sorption capacity, should be carefully addressed. For these reasons, selecting appropriate materials for heavy metal ion sorption from an aqueous medium is critical. Adsorbents such as zeolites, polymers, metal oxides, and polymer/metal oxides have been used as materials for the sorption of heavy metal ions. From these promising adsorbents, poly (vinyl alcohol) PVA is identified to be associated with various organic and inorganic compounds able to supply hydroxyl groups on its surface for the elimination of heavy metal ions. Because of its unique features such as high porosity, large surface area, and tiny pore size, it has been widely employed for heavy metal ion adsorption. Furthermore, it provides a greater possibility for nanoparticle loading without affecting mechanical stability [25–27].

Metal oxide nanoparticles placed inside a polymer matrix have recently piqued the interest of researchers due to the unique features of hybrid nanocomposites. Many factors influence the properties of the created nanocomposites, including the synthesis method, its morphological structure, the characteristics of the metal oxide nanoparticles that are implemented in PVA, and the physicochemical properties of both metal oxide and polymer molecules in the interaction [28–30]. One of these techniques, that helped us to vary the characteristics of embedding metal oxide in a simple way, is the pulsed laser ablation in liquid media approach. It is a simple, quick, economical, green, dependable method for producing a wide range of nanostructured materials and a commonly used technology for producing nanocomposite adsorbent materials that has received a lot of attention recently. This method allows us to produce nanostructured materials in high purity without any minor products as it is based on using just required precursor pure metals not in their salts at the beginning of the preparation, and it did not require surfactants to preserve the size in nanoscale form. Furthermore, the normal behavior of the preparation of nanostructured materials via any physical or chemical approach methods is associated with the generation of hazard vapor fumes consisting of very finer powders from the prepared nanostructured form, which have a very dangerous side effect on the environment and human health as they are capable of passing through human skin, while in this method, all the preparation steps were carried out inside a liquid medium, which prevents the transfer of any vapor fumes to the environment or human bodies. Therefore, this method could be considered an *eco-friendly* and green method. Furthermore, this method is eligible to form nanocomposite structures by ablating many metal targets at the same time or changing the liquid media with a matrix structure, such as PVA or CNTs. Therefore, this method fits the need for versatility, which affects the shape and size of the produced nanostructured materials in comparison to other methods. However, this mass production of this method could represent the main issue faced by the enhancement and development of this method [31–35]. The achievement of the PLAL method in the preparation of Al_2O_3 NPs could be summarized as follows: In 2010, S. Khan et al. studied the effect of the ablation time of the continuous

wave (CW) of fiber laser to obtain Al_2O_3 NPs with different particle sizes [36]. In 2012, V. Piriya Wong et al. prepared Al_2O_3 NPs by ablating Al pellet immersed in deionized water. It was shown that their particle size could be changed by varying the ablation energy [37]. In 2020, A. Riahi et al. showed the prepared Al_2O_3 NPs by laser ablation (7 ns, 1064 nm, and 120 mJ) of Al target immersed in deionized water with have high thermal conductivity [38]. Moreover, M. Eskandari et al. prepared $\text{Au@Al}_2\text{O}_3$ core-shell in just one step by ablating bulk aluminum deposited with a thin layer from the Au layer immersed in ethanol solution by CW fiber laser (1064 and 40 W). This preparation method could be represented the development of the PLAL method for generating core/shell nanocomposite structures [39]. Furthermore, A. Mostafa et al. showed the capability for preparing different metal oxides embedded in PVA structure in just a one-pot method by ablating metal plates (Al, Cd, and Cu) in PVA solution [40]. Moreover, A. Mostafa et al. showed another facility laser parameter to enhance the PLAL method, by making laser irradiation after the laser ablation process to decrease the particle size of the prepared Al_2O_3 NPs [41]. Furthermore, the previous contributions of Al_2O_3 -PVA nanocomposite for the removal of heavy metals or degraded organic pollutants can be summarized in Table 1.

Table 1. Recent survey of nanocomposite based on Al_2O_3 -PVA for removal heavy metals or degradation of organic pollutants.

Composite	Organic Pollutants/Heavy Metals	Efficacy
Al_2O_3 -PVA [42]	phosphate	95%
PVA-ZnO- Al_2O_3 [43]	MB	100%
Polythiophene/PVA/ Al_2O_3 [44]	Pb(II),	97.3%
	Zn(II),	89.4%
	Cd(II)	95.8%
Polyaniline/PVA/ Al_2O_3 [44]	Pb(II),	89.78%
	Zn(II),	84.9%
	Cd(II)	79.2%

In this work, an Al_2O_3 -PVA nanocomposite was effectively produced in just one step using the *eco*-friendly promising tools of the PLAL method to be suitable for nickel ion adsorption from aqueous solutions. The properties of the synthesized hybrid structure were carried out by different techniques. After that, the influence of several factors on the sorption process, such as concentration, contact duration, beginning concentration, and temperature was examined for Ni(II).

2. Materials and Experimental Work

2.1. Materials

Ultra-pure water was used to make all of the reagents. Poly vinyl alcohol solution (PVA) was purchased from La-113 laboratory, Rasayan, Egypt. Aluminum sheet (Al) with dimension $2 \times 2 \text{ cm}^2$ and thickness of 0.1 mm was purchased from the BDH Chemical Ltd. pool, England. Nickel nitrate (NiNO_3) was purchased from LOBA Chemie, Laboratory Reagents and fine Chemicals, India, which was used to make a stock solution of Ni(II) ions. Sodium hydroxide (NaOH) and hydrochloric acid (HCl) were purchased from El Nasr Pharmaceutical Co., Giza, Egypt.

2.2. Preparation of PVA Solution

A 10 wt.% PVA was produced by dissolving 10 g of PVA in 100 mL of ultra-pure water and maintaining it at 80°C for 300 min with continued magnetic stirring.

2.3. Preparation of Al_2O_3 -PVA Composite

The Al_2O_3 nanostructured material was generated by the pulsed laser ablation of cleaned metal targets of Al sheet put in a glass vessel filled with 5 mL of the prepared PVA

solution to form an Al_2O_3 nanostructured material embedding PVA. The laser ablation process produced by the laser beam of the first harmonic generation of nanosecond Nd:YAG laser, which produces a 10 Hz repetition rate and 150 mJ of laser energy. The ablation process was carried out by focusing the laser beam on the target's surface with a plano-convex lens (70 mm) to produce a small spot that had a 20 μm diameter (Figure 1). The ablation procedure was carried out under mechanical stirring for 30 min to create distinct nanocomposite structures. Then, the prepared nanocomposite solution was separately cast in a glass Petri-dish to obtain the required films, followed by drying in glass Petri dishes with a thickness of about 2 mm in the form of free-standing and a diameter of 25 mm. The amount of immobilized Al_2O_3 NPs in PVA could be estimated in two ways: the first method was related to measuring the weight of the Al-sheet before and after the ablation process, followed by subtraction of the two values ($\text{weight}_{\text{Al sheet}} - \text{weight}_{\text{ablated Al sheet}}$) to estimate the amount of immobilized Al_2O_3 NPs in PVA. The second method was related to measuring the weight of PVA film before and after being embedded with Al_2O_3 NPs, followed by subtraction of the two values ($\text{weight}_{\text{embedded PVA film}} - \text{weight}_{\text{pure PVA film}}$) to estimate the amount of immobilized Al_2O_3 NPs in PVA. After using both methods and repeating each method three times, it was detected that the amount of embedded Al_2O_3 in the PVA film is $9.2 \mu\text{g} \pm 0.051$.

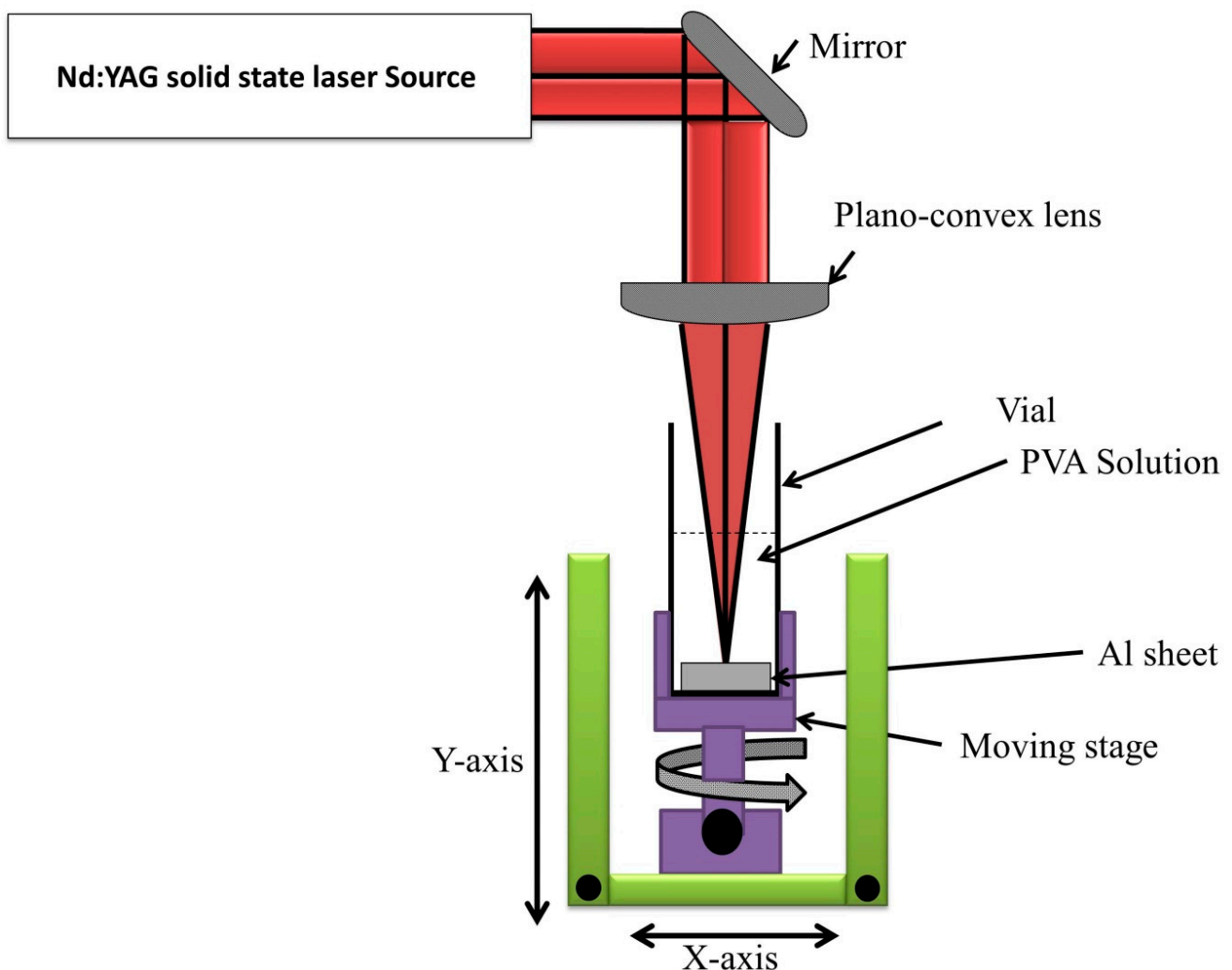


Figure 1. Schematic diagram of Al_2O_3 -PVA nanocomposite by PLAL.

2.4. Investigation Techniques

X-ray diffractometer (Shimadzu XRD 7000, Kyoto, Japan), UV–VIS–NIR spectrophotometer (JASCO 570 UV–VIS–NIR, Kyoto, Japan), atomic absorption spectroscopy (Shimadzu AA-6200; Shimadzu Co., Ltd., Kyoto, Japan), FT-IR (JASCO FT-IR 6100 spectrometer, Japan), and a scanning electron microscope associated with EDX analyzer detector (PHILIPS/FEI QUANTA 250, Prague, Czech Republic).

2.5. Adsorption Study

The batch sorption of Ni(II) ions onto a PVA–Al₂O₃ nanocomposite adsorbent in aqueous solutions at ambient temperature was examined. For that, a conical flask containing 100 mL of Ni²⁺ metal ion solution was filled with ultra-pure water and stirred to achieve an initial Ni solution concentration ranging from 10 to 100 mg/L before being put in a thermostatic shaker for adsorption (200 rpm). The remaining Ni²⁺ ion concentration was then measured using atomic absorption spectroscopy. The following formulae were used to investigate the effect of various parameters on the adsorption capacity of Ni²⁺ [45,46].

$$\text{Removal extent, percentage} = (C_0 - C_a)/C_0 \times 100 \quad (1)$$

where C₀ and C_a are the concentrations of adsorbent material at the beginning of the adsorption process and at the equilibrium of the adsorption process, respectively.

3. Result and Discussion

3.1. Investigation of the Prepared Al₂O₃-PVA Nanocomposite

Figure 2 shows the FT-IR spectra of PVA, Al₂O₃ nanoparticles, and Al₂O₃-PVA nanocomposite to identify their vibrational absorption motion, which is produced by FT-IR spectra. The FT-IR spectra of pure PVA exhibited a strong and wide stretching band at 3334 cm⁻¹ and a bending vibration at 1565 cm⁻¹, 1428 cm⁻¹, and 1325 cm⁻¹ that can be attributed to the hydroxyl group because of intramolecular and intermolecular hydrogen bonding. Furthermore, stretching vibrational absorption bands at 2945 cm⁻¹ and 2908 cm⁻¹ appeared as a result of functional groups of the CH and –CH₂ groups, respectively. Furthermore, the appearance of stretching vibration around 1100 cm⁻¹ was related to the C–O functional group. These characteristics could be represented by the main functional groups of the PVA structure. In addition to the appearance of a vibrational stretching peak around 1739 cm⁻¹ related to the C=O functional group, but with small intensity as it was related to the presence of leftover acetate groups after the hydrolysis of polyvinyl acetate to produce PVA [30,47,48]. In the case of the laser ablation of the Al sheet immersed in the ultra-pure water, the FT-IR spectra of Al₂O₃ nanoparticles exhibited two distinctive vibrational peaks of Al₂O₃, at 558 cm⁻¹ and 632 cm⁻¹, which are exhibited in the fingerprint region. Furthermore, the appearance of vibrational peaks characterized by a broad band stretching motion around 3342 cm⁻¹ was related to the residual hydroxyl functional group (–OH) that was produced by atmospheric moisture. Moreover, there are no other peaks related to the residual organic compounds. In the case of Al₂O₃-PVA nanocomposite, the primary distinctive vibrational peaks of the PVA structure are still intact, but their strength and position have changed. The intensity of these hydroxyl group bands is clearly reduced, which is attributable to the interaction of the PVA structure with Al ions. Moreover, below 1000 cm⁻¹, there are two distinct peaks of Al₂O₃, at 558 cm⁻¹ and 632 cm⁻¹, which are exhibited in the fingerprint area of the spectra as evidence for the incorporation of Al₂O₃ molecules in the polymer matrix. Moreover, it was clear that the strong electronegativity of the atoms formed from Al₂O₃ and injected into the polymeric matrix of PVA structure, which has a significant impact on the spectrum of adjacent group frequencies, may be responsible for the conformational changes in the width and intensity of the vibrational bands of PVA structure [20,41,49]. These significant fluctuations in the absorbance and frequencies of almost bands suggest that interactions between Al₂O₃ NPs and the polymeric structure of PVA, such as hydrogen bonds or van der Waals interac-

tions, are forming between the $(\text{OH}^-)/(\text{COO}^-)$ groups of PVA and the Al_2O_3 NPs. This was accomplished by reducing the crystallinity degree of nanocomposites and forming charge transfer complexes in which the Al_2O_3 NPs function as an electron acceptor and the PVA matrix works as an electron donor. These interactions alter the dynamics of the nanocomposite chain structure.

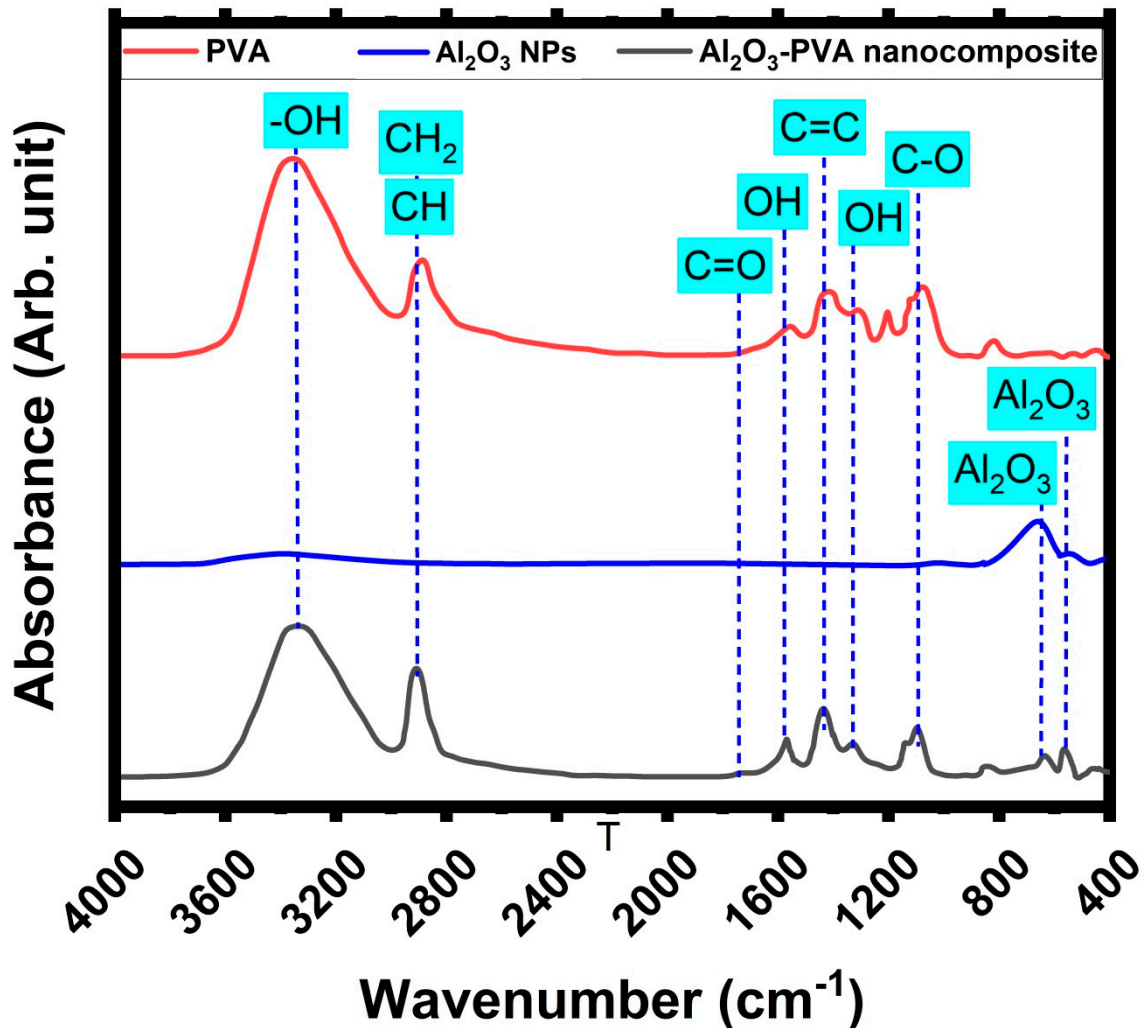


Figure 2. FT-IR spectra of PVA, Al_2O_3 nanoparticles, and $\text{Al}_2\text{O}_3/\text{PVA}$ nanocomposite.

FESEM was used to investigate the morphological changes in PVA caused by embedding with Al_2O_3 molecules as mentioned in Figure 3. The micrographs exhibit SEM of Al_2O_3 nanoparticles, PVA, and the hybrid with PVA- Al_2O_3 nanocomposite. The surface of the produced structure from the laser ablation of the Al sheet in the ultra-pure water showed a semi-spherical shape in the nanoscale form, while the SEM image of the PVA structure showed a uniform surface shape that reveals dispersed smooth microspores instead of uniform ones. Moreover, the surface of the polymer was significantly distorted during metal oxide contact, and the metal oxide particles were uniformly dispersed over the polymer surface compared to the pure PVA structure. As a result, the change in the surface of the PVA- Al_2O_3 nanocomposite reveals that the PVA surface was highly deformed, and the aluminum oxides were homogeneously distributed throughout the PVA surface.

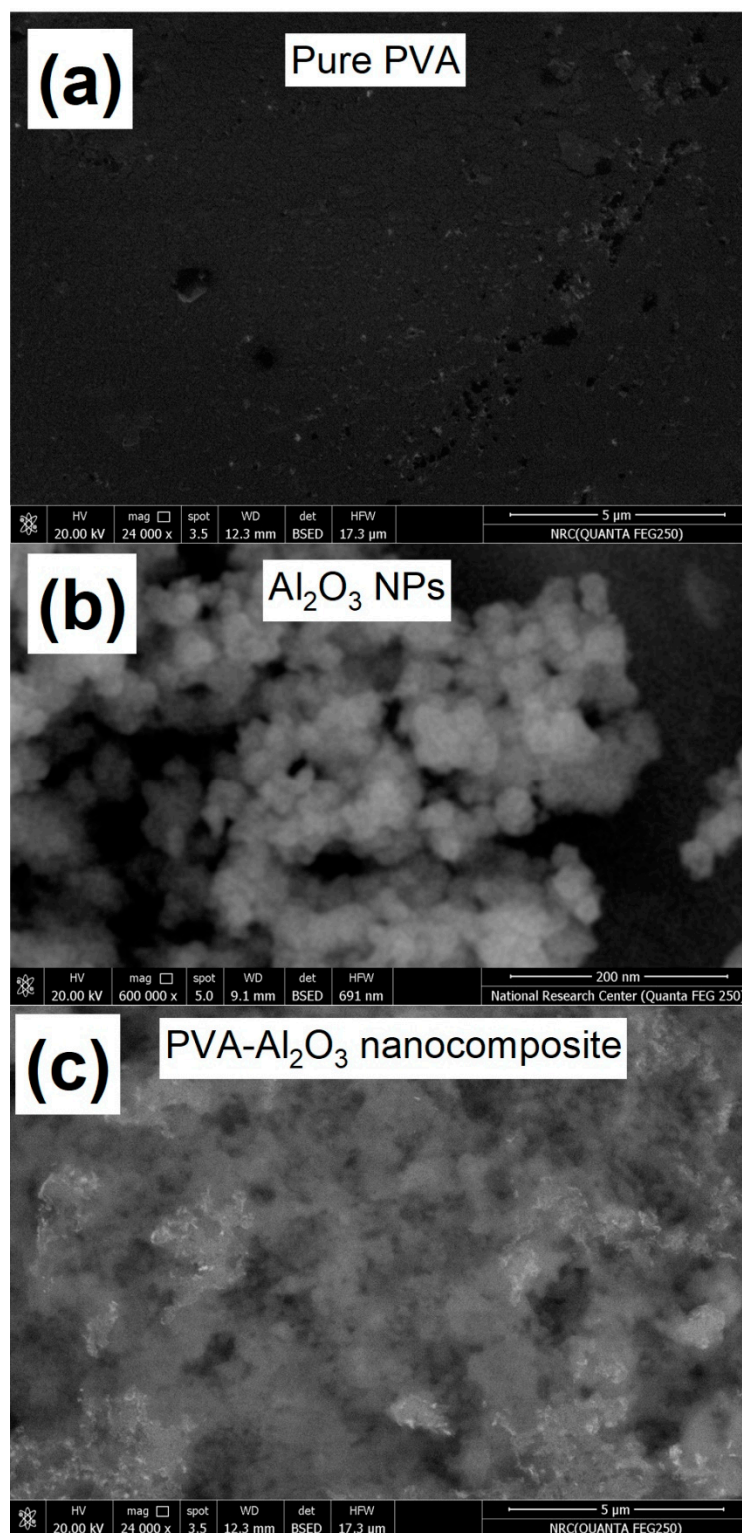


Figure 3. SEM image of (a) PVA, (b) Al₂O₃ nanoparticles, and (c) Al₂O₃/PVA nanocomposite.

Furthermore, the elements on the surface of the PVA structure before and after embedding with Al₂O₃ NPs were examined using an EDX element analyzer. Figure 4 depicts the EDX spectra of a PVA-Al₂O₃ nanocomposite before and after Al₂O₃ NPs adsorption. This result verified the presence of a pure PVA structure as it was only comprised of the C and O elements, which represented the main constituted elements of the PVA structure. Moreover, the elemental analysis confirmed the formation of pure Al₂O₃ nanoparticles

from the laser ablation process in the ultra-pure water as it was only comprised of the Al and O elements, which represented the main constituted elements of the Al_2O_3 structure. However, in the case of embedding with Al_2O_3 , a new element (Al) was injected with C and O. So, the PVA structure was embedded with the Al element. Moreover, the phase of Al could be detected to be metallic or oxide form based on looking at the ratio of O/C in PVA structure before and after ablation of Al, which was 0.797 and 1.42, respectively. So, the amount of O was increased owing to the occurrence of Al in the oxide form (Al_2O_3).

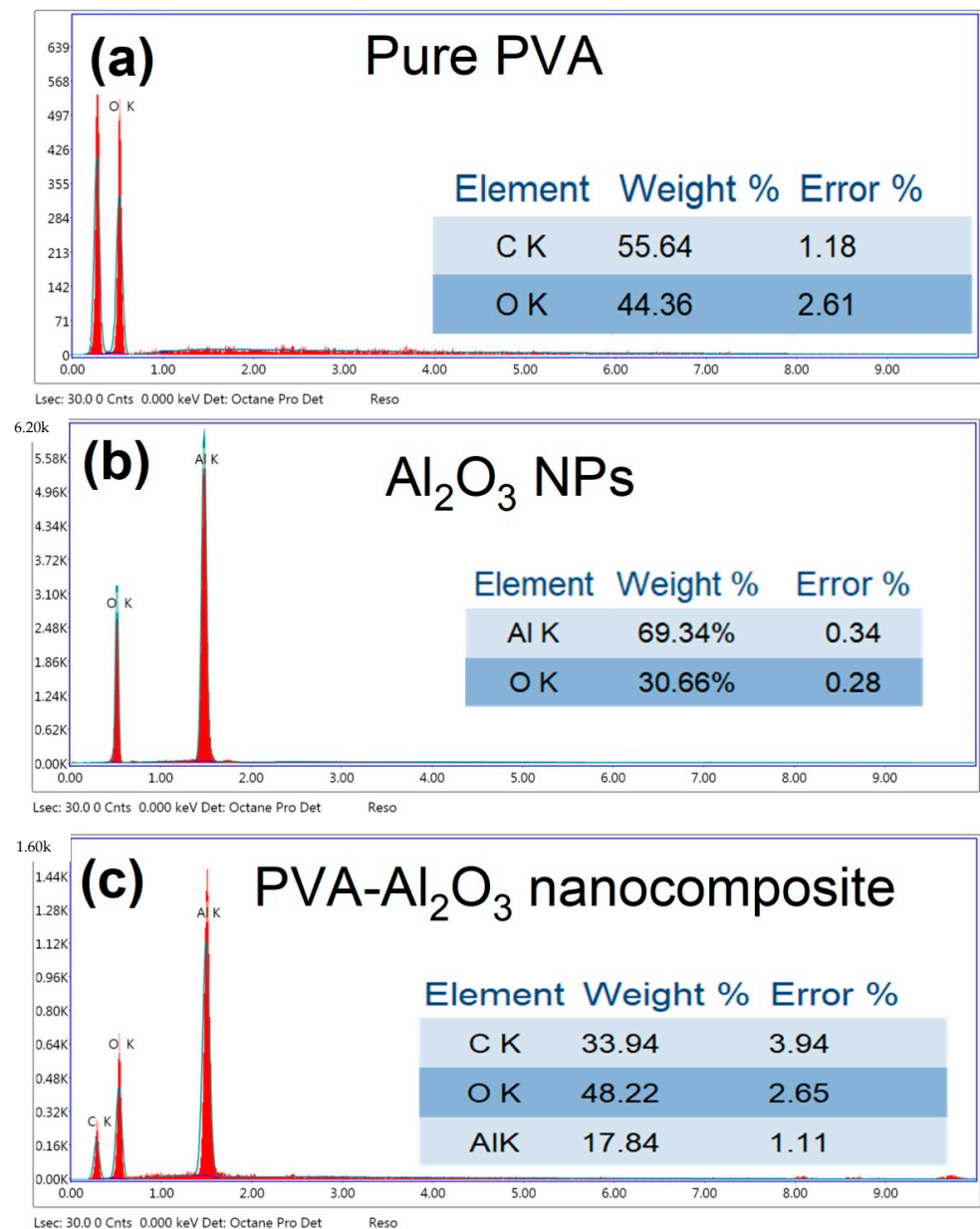


Figure 4. EDX elemental analysis of (a) PVA and (b) EDX elemental analysis of PVA before and (c) after embedding with Al_2O_3 .

The XRD measurements were used to examine the crystallinity of the PVA structure with and without incorporated metal produced from the laser ablation of the Al sheet. Nanostructured materials were created by the PLAL method of an Al target immersed in different types of liquid media, and the resultant diffractogram spectra are given in Figure 5. In the case of pure PVA, there are two separate diffraction peaks at diffraction angles $2\theta = 19.5^\circ$ and 40.5° , which correspond to the indices planes (1 0 1) and (1 1 1),

respectively [50]. Furthermore, no other peaks were observed related to any foreign impurities in the PVA structure.

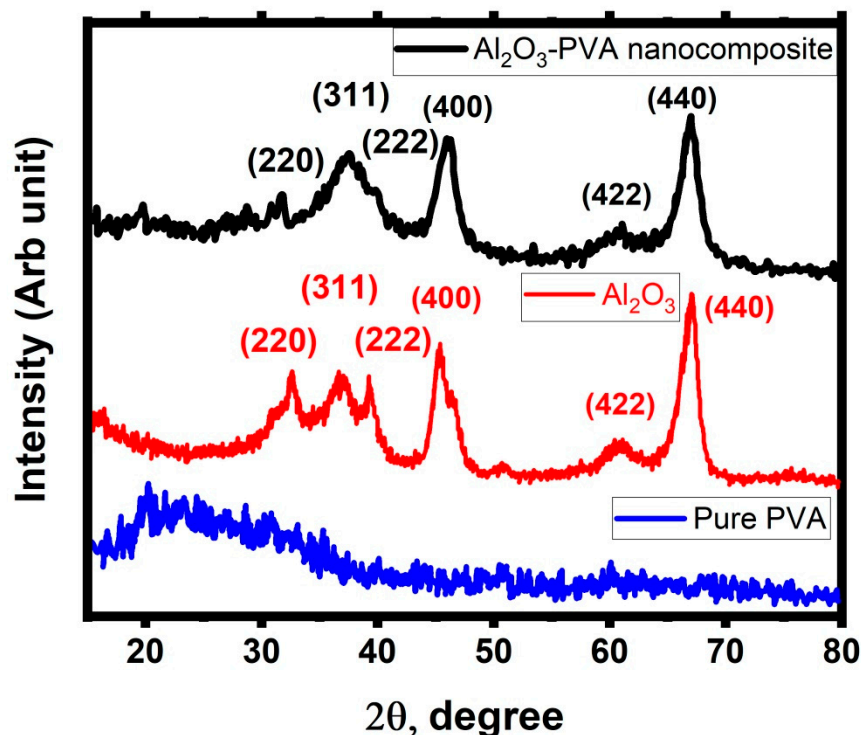


Figure 5. XRD diffractogram of PVA, Al₂O₃ nanoparticles, and Al₂O₃/PVA nanocomposite.

In the case of the laser ablation of the Al sheet immersed in the ultra-pure water, the crystalline peaks appeared at 31.62°, 37.18°, 39.79°, 46.17°, 60.84°, and 67.13°, which correspond to (2 2 0), (3 1 1), (2 2 2), (4 0 0), (4 2 2), and (4 4 0), respectively, based on JCPD XRD card number 79-1558 of the cubic structure of Al₂O₃. Moreover, no other typical peaks were seen in the diffractogram, which may be produced from the other contaminants during the preparation steps. This observation confirmed the high purity of the produced nanostructure materials. Moreover, the main crystalline peak used to detect the crystallite size of Al₂O₃ nanostructure using the Debye–scherrer equation [51].

$$D = \frac{0.9\lambda}{\beta \cos \theta} \tag{2}$$

where D , λ , β , and θ are the crystallite size of Al₂O₃ nanostructure, used X-ray wavelength, FWHM of the diffraction peak at $2\theta = 67.13^\circ$, and the Bragg angle (33.57°), respectively, its crystallite is 19.8 nm. In the case of laser ablation of Al sheet immersed in the PVA solution, the semi-crystalline structure was still present in the case of embedding with the generated nanostructured materials formed from the PLAL process of Al-target immersed in PVA solution, but the intensity was reduced by a large amount under the effect of the intermolecular hydrogen band produced between the PVA structure and nanostructured materials. Furthermore, the new crystalline peaks appeared at 31.62°, 37.18°, 39.79°, 46.17°, 60.84°, and 67.13°, which correspond to (2 2 0), (3 1 1), (2 2 2), (4 0 0), (4 2 2), and (4 4 0), respectively, based on JCPD XRD card number 79-1558 of the cubic structure of Al₂O₃ [52]. It was clear that the PVA diffraction peaks remained after being incorporated with Al₂O₃ NPs in the creation of a nanocomposite structure. It was demonstrated that the Al₂O₃ NPs incorporation had no effect on the distribution of the PVA’s crystallinity, while its area under the curve has changed to a lower value, indicating that the crystallinity of the PVA structure has reduced. This reduction could be related to the presence of intermolecular hydrogen bonding that occurred between its chain structure and Al₂O₃ NPs, leading

to reducing the intermolecular interaction between the chains of PVA. Therefore, the electrostatic interaction of Al₂O₃ NPs with the PVA chain leads to disturbing the crystalline phase of the PVA structure. So, this observation could be represented as a confirmation of successful incorporation.

3.2. Adsorption Process

3.2.1. Effect of pH

The pH of the solution is a critical variable in the adsorption process because it influences metal sorption via protonation and deprotonation of the adsorbent's functional groups, the Ni speciation, adsorbent surface charge, and adsorbent ionization. As a result, the influence of pH on nickel sorption is explored in the pH range 2–7 for an initial concentration of 100 mg L⁻¹ from Ni(II), an adsorbent dose of 0.5 g/L, and a temperature of study at 303 K as depicted in Figure 6a. This graph clearly shows that the adsorption capacity rises with a rising pH value, and the precipitation occurs in nickel solutions when the pH exceeds 7. So, the trials are not undertaken above a pH of 7. Furthermore, around pH 5.3, nickel adsorption capacity reaches a maximum of 62 mg g⁻¹ and thereafter decreases with increasing pH levels [53–56]. This was related to:

1. At pH values higher than 6, the excess of alkaline –OH group has a greater tendency to combine with Ni²⁺ and form Ni(OH)₂ participated, causing the adsorption to be diminished.
2. At pH values in the range 5–6, the surface charge of the hybrid nanocomposite turned to a negative charge due to the medium having a low acidic concentration, increasing the coordination between positively charged metal ions (Ni²⁺) and Al₂O₃-PVA nanocomposite by electrostatic attraction, leading to reach the maximum adsorption capacity. The results were consistent with Ni²⁺ adsorption on Al₂O₃-PVA nanocomposite as mentioned in the previous work [57].
3. At pH values lower than 5, the decrease in nickel adsorption capability at lower pH levels is related to protonation of the Al₂O₃-PVA nanocomposite by the acidic medium and the water molecules converted from H₂O to H₃O⁺, leading to a decrease in the number of charge carriers in the hybrid membrane for metal adsorption. In addition, competition for adsorption sites on the PVA structure created between H⁺ and Al²⁺ make an electrostatic repulsion between them [58–61].

3.2.2. Effect of Initial Pollutant Concentration

The influence of initial Ni²⁺ concentrations on nanocomposite adsorption was examined from 0 mgL⁻¹ to 500 mgL⁻¹ of beginning Ni(II) concentration at a temperature of study at 303 K, pH 5.3, and an adsorbent dose of 0.5 g/L, and the findings are presented in Figure 6b. It was shown that the initial Ni²⁺ concentration in aqueous solution increased till it reached saturation and then decreased. So, the precision description of this process can be described as the percentage amount of Ni(II) removal greatly reduced as the beginning Ni(II) ion concentration content rises. This observation could be discussed when the initial Ni(II) ion concentration increased from 0 to 200 mg/L, the mass transfer of Ni(II) ions between the aqueous solution and the Al₂O₃ nanoparticles were supported, leading to improved interaction between Ni(II) ions and the Al₂O₃ nanoparticles and increasing the adsorption uptake of Ni(II). In other words, when the initial Ni(II) ion concentration was further increased from 200 to 500 mg/L, the adsorption capacity hit a plateau due to the strong binding sites on the Al₂O₃/PVA nanocomposites have been filled with the initial amounts of Ni(II) ions, which appeared from the adsorption isotherm analysis as the Langmuir and Freundlich models, which were compatible with the other scholars who had observed similar findings. So, from this study, the optimum beginning Ni(II) ion concentration for a good adsorption process was chosen before the plateau shape, at 100 mg/L as this value represented the highest rate of adsorption capacity and after this value, the rate of adsorption capacity started to be decreased [62–64].

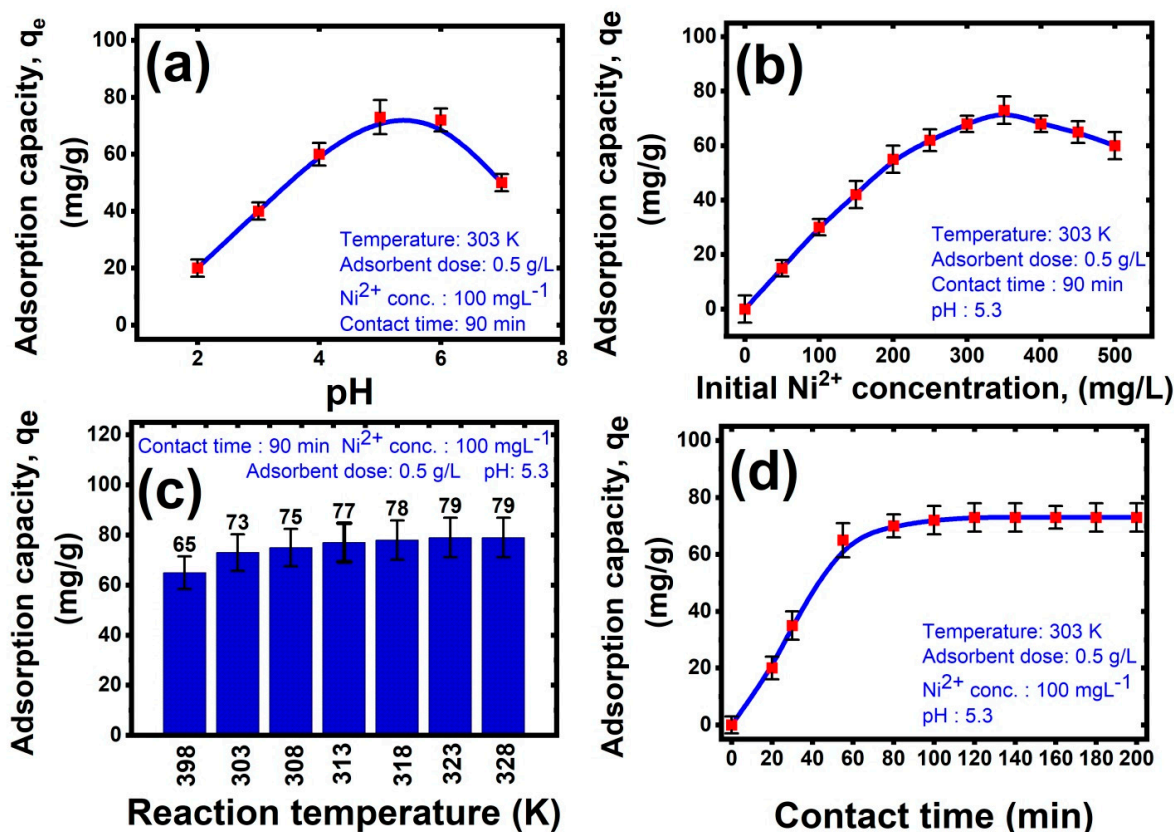


Figure 6. Effect of (a) pH, (b) beginning Ni²⁺ concentration, (c) reaction temperature, and (d) contact time on Ni(II) removal by Al₂O₃/PVA nanocomposite.

3.2.3. Effect of Temperature

Figure 6c depicts the influence of reaction temperature on the removal of Ni²⁺ ions for 100 mg L⁻¹ beginning Ni(II) ion concentration, an adsorbent dose of 0.5 g/L, and pH of 5.3 for nickel solutions at varying temperatures from 298 K to 328 K. As the temperature rose from 298 to 328 K, the adsorption capacity of nickel ions grew from 65.8 mg g⁻¹ to 87.4 mg g⁻¹. These findings revealed that nickel ion sorption onto the Al₂O₃/PVA nanocomposite adsorbent was endothermic.

3.2.4. Effect of Contact Time

Figure 6d depicts the influence of contact time on the removal of Ni²⁺ ions for starting metal concentrations of 0 and 500 mgL⁻¹, an adsorbent dose of 0.1 g/L, an adsorbent dose of 0.5 g/L, and pH of 5.3 for nickel solutions at 303 K temperature. At varied starting metal concentrations of 0 and 100 ppm, the adsorption efficiency for nickel ions by the Al₂O₃/PVA nanocomposite rose dramatically and achieved equilibrium after 90 min. As a result, a time of 50 min was chosen as an equilibrium time for future tests. Furthermore, as demonstrated, the sorption capacity of Al₂O₃/PVA nanocomposite increases with time due to the increased diffusivity of nickel ions toward Al₂O₃/PVA nanocomposite [65].

3.3. Mechanism of Adsorption Process

The adsorption of metal ions of Ni²⁺ by the nanocomposite could be controlled in three ways. The first predicted mechanism was the nanocomposite adsorbent’s quick transfer to the external surface absorption of metal ions. The second predicted mechanism was the diffusion of metal ions via the pores of the nanocomposite. The third predicted mechanism might be linked to chemical adsorption between nanocomposite functional groups, such as hydroxyl groups, and metal ions. The experimental results were analyzed using pseudo-

first-order or pseudo-second-order kinetic models to study the kinetic parameters of the adsorption of metal ions via the Al₂O₃/PVA nanocomposite [30,66–68].

$$q_t = q_e (1 - e^{-k_1 t}) \text{ Pseudo-first-order} \tag{3}$$

$$q_t = (k_2 q_e^2 t) / (1 + q_e k_2 t) \text{ Pseudo-second-order} \tag{4}$$

where q_t is the amount of adsorbed metal after t time, q_e is the amount of adsorbed metal after equilibrium time, k_1 is the constant of pseudo-first-order, and k_2 is the constant of pseudo-second-order. From Figure 7, the intercept, slope, and the correlation coefficient of Pseudo-first-order are 4.95347 ± 0.03878 , -0.3606 ± 0.00983 , and 0.98969 , respectively, while the intercept, slope, and the correlation coefficient of Pseudo-second-order are 0.15013 ± 0.00719 , $0.01219 \pm 8.87805 \times 10^{-5}$, and 0.99926 , respectively. So, the value of k_1 and k_2 are 0.3606 and $9.9 \times 10^{-4} \text{ gmg}^{-1} \text{ min}^{-1}$, respectively. Therefore, in the case of the pseudo second-order, the predicted equilibrium adsorption capacity was more compatible with its experimental value.

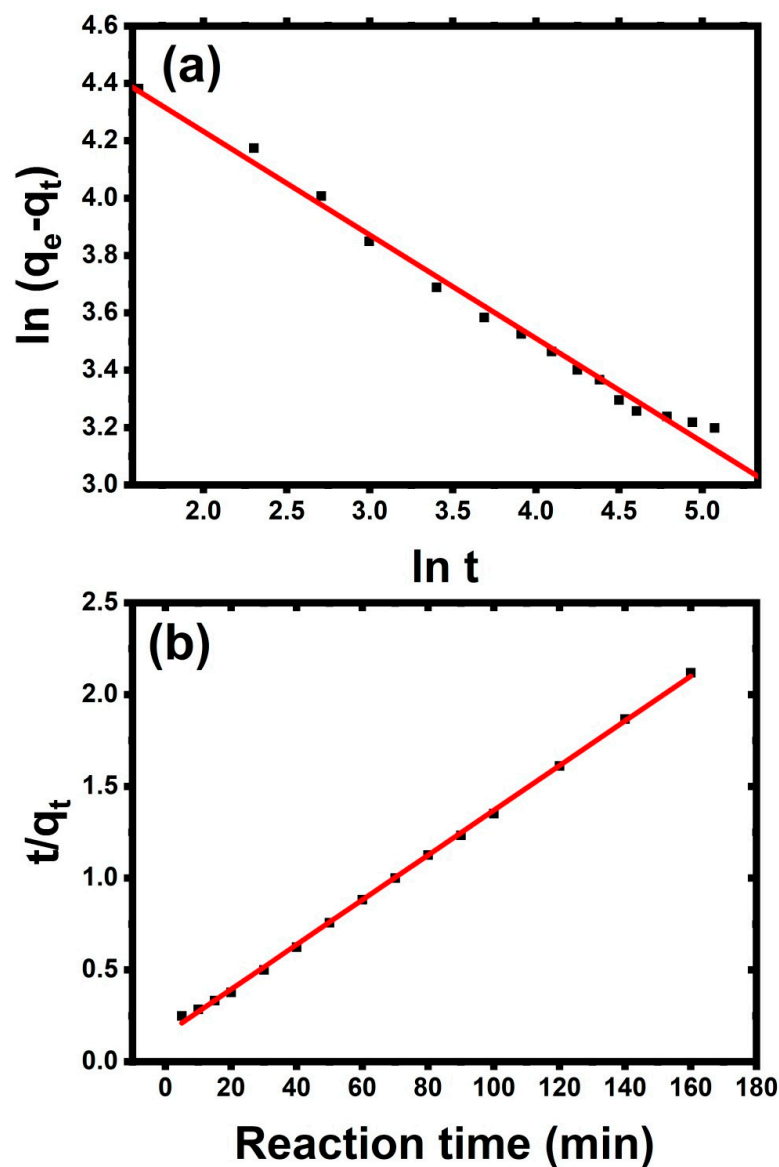


Figure 7. Adsorption kinetics of Ni(II) ions by Al₂O₃/PVA nanocomposite (a) Pseudo-first-order and (b) Pseudo-second-order.

4. Conclusions

A novel hybrid PVA/Al₂O₃ nanocomposite was created in this study using a simple green potential approach. This approach used a pulsed laser ablation method to create a hybrid nanocomposite from an Al sheet immersed in PVA solution. The successful embedding of PVA structure with Al₂O₃ nanoparticles was demonstrated by FTIR, XRD, and SEM-EDAX investigation of PVA before and after contact with Al₂O₃ nanoparticles. It can be utilized as a cost-effective alternative to activated carbons, membrane filtration, and ion-exchange adsorbents. The adsorbent effectively removes Ni(II) from aqueous solutions, with even greater removal achieved at low concentrations of about 100 mg/L. The adsorption was shown to be pH-dependent, with pH 5.3 yielding the most clearance. The pseudo-second-order rate kinetics was used to manage the removal process. The adsorption findings revealed that hybrid PVA/Al₂O₃ nanocomposite may be utilized to efficiently remove Ni(II) from aqueous solutions.

Author Contributions: Conceptualization, A.M.M., F.H.A. and E.A.M.; methodology, S.H.A., E.A., E.A.M. and F.H.A.; software, H.A.A., T.A.A., F.H.A. and A.M.M.; formal analysis, A.M.M. and H.A.A.; investigation, A.M.M., R.A.P., S.H.A., E.A. and E.A.M.; resources, T.A.A., A.B.G.T. and F.H.A.; data curation, H.A.A.; writing—original draft preparation, A.M.M., E.A.M. and H.A.A.; writing—review and editing, F.H.A. and R.A.P.; supervision, A.M.M.; project administration, A.M.M. and F.H.A.; funding acquisition, F.H.A. All authors have read and agreed to the published version of the manuscript.

Funding: This research was funded by Princess Nourah bint Abdulrahman University Researchers Supporting Project number (PNURSP2022R38), Princess Nourah bint Abdulrahman University, Riyadh, Saudi Arabia.

Institutional Review Board Statement: Not Applicable.

Informed Consent Statement: Not Applicable.

Data Availability Statement: Not Applicable.

Acknowledgments: The authors express their gratitude to Princess Nourah bint Abdulrahman University Researchers Supporting Project number (PNURSP2022R38), Princess Nourah bint Abdulrahman University, Riyadh, Saudi Arabia. Also, the authors would like to thank the Deanship of Scientific Research at Umm Al-Qura University for supporting this work by Grant Code: (22UQU4320141DSR09).

Conflicts of Interest: The authors declare no conflict of interest.

References

1. Altowyan, A.S.; Toghan, A.; Ahmed, H.A.; Pashameah, R.A.; Mwafy, E.A.; Alrefae, S.H.; Mostafa, A.M. Removal of methylene blue dye from aqueous solution using carbon nanotubes decorated by nickel oxide nanoparticles via pulsed laser ablation method. *Radiat. Phys. Chem.* **2022**, *198*, 110268. [[CrossRef](#)]
2. Al-Kadhi, N.S.; Pashameah, R.A.; Ahmed, H.A.; Alrefae, S.H.; Alamro, F.S.; Faqih, H.H.; Mwafy, E.A.; Mostafa, A.M. Preparation of NiO/MWCNTs nanocomposite and its application for cadmium ion removal from aqueous solutions. *J. Mater. Res. Technol.* **2022**, *19*, 1961–1971. [[CrossRef](#)]
3. Mwafy, E.A.; Mostafa, A.M. Tailored MWCNTs/SnO₂ decorated cellulose nanofiber adsorbent for the removal of Cu (II) from waste water. *Radiat. Phys. Chem.* **2020**, *177*, 109172. [[CrossRef](#)]
4. Alkallas, F.H.; Toghan, A.; Ahmed, H.A.; Alrefae, S.H.; Pashameah, R.A.; Alrebdi, T.A.; Mwafy, E.A.; Mostafa, A.M. Catalytic performance of NiO nanoparticles decorated carbon nanotubes via one-pot laser ablation method against methyl orange dye. *J. Mater. Res. Technol.* **2022**, *18*, 3336–3346. [[CrossRef](#)]
5. Jaleh, B.; Nasrollahzadeh, M.; Mohazzab, B.F.; Eslamipannah, M.; Sajjadi, M.; Ghafuri, H. State-of-the-art technology: Recent investigations on laser-mediated synthesis of nanocomposites for environmental remediation. *Ceram. Int.* **2021**, *47*, 10389–10425. [[CrossRef](#)]
6. Yu, B.; Chen, Y. Conductive WO₃-x@CNT networks for efficient Li-S batteries. *IOP Conf. Ser. Mater. Sci. Eng.* **2020**, *892*, 012027. [[CrossRef](#)]
7. Chen, J.; Wu, X.; Tan, Q.; Chen, Y. Designed synthesis of ultrafine NiO nanocrystals bonded on a three dimensional graphene framework for high-capacity lithium-ion batteries. *New J. Chem.* **2018**, *42*, 9901–9910. [[CrossRef](#)]

8. Zhang, Z.; Zhang, X.; You, X.; Zhang, M.; Walle, M.D.; Wang, J.; Li, Y.; Liu, Y.-N. 3D well-interconnected NiO–graphene–carbon nanotube nanohybrids as high-performance anode materials for Li-ion batteries. *J. Nanopart. Res.* **2016**, *18*, 247. [[CrossRef](#)]
9. Li, T.; Ni, S.; Lv, X.; Yang, X.; Duan, S. Preparation of NiO–Ni/natural graphite composite anode for lithium ion batteries. *J. Alloy. Compd.* **2013**, *553*, 167–171. [[CrossRef](#)]
10. Xiao, J.; Huang, J.; Wang, M.; Huang, M.; Wang, Y. The fate and long-term toxic effects of NiO nanoparticles at environmental concentration in constructed wetland: Enzyme activity, microbial property, metabolic pathway and functional genes. *J. Hazard. Mater.* **2021**, *413*, 125295. [[CrossRef](#)]
11. Oliveira, A.R.; Correia, A.A.; Rasteiro, M.G. Heavy Metals Removal from Aqueous Solutions by Multiwall Carbon Nanotubes: Effect of MWCNTs Dispersion. *Nanomaterials* **2021**, *11*, 2082. [[CrossRef](#)] [[PubMed](#)]
12. Egbosiuba, T.C.; Abdulkareem, A.S.; Kovo, A.S.; Afolabi, E.A.; Tijani, J.O.; Bankole, M.T.; Bo, S.; Roos, W.D. Adsorption of Cr(VI), Ni(II), Fe(II) and Cd(II) ions by KIAGNPs decorated MWCNTs in a batch and fixed bed process. *Sci. Rep.* **2021**, *11*, 75. [[CrossRef](#)] [[PubMed](#)]
13. Carolin, C.F.; Kumar, P.S.; Saravanan, A.; Joshiba, G.J.; Naushad, M. Efficient techniques for the removal of toxic heavy metals from aquatic environment: A review. *J. Environ. Chem. Eng.* **2017**, *5*, 2782–2799. [[CrossRef](#)]
14. Soltani, R.; Pelalak, R.; Pishnamazi, M.; Marjani, A.; Albadarin, A.B.; Sarkar, S.M.; Shirazian, S. A novel and facile green synthesis method to prepare LDH/MOF nanocomposite for removal of Cd(II) and Pb(II). *Sci. Rep.* **2021**, *11*, 1609. [[CrossRef](#)]
15. Arsalani, N.; Bazazi, S.; Abuali, M.; Jodeyri, S. A new method for preparing ZnO/CNT nanocomposites with enhanced photocatalytic degradation of malachite green under visible light. *J. Photochem. Photobiol. A Chem.* **2020**, *389*, 112207. [[CrossRef](#)]
16. Hareesh, K.; Sunitha, D.V.; Dhole, S.D.; Bhoraskar, V.N.; Phase, D.M.; Williams, J. One-step gamma radiation aided diffusion of Ag–Au alloy nanoparticles into polycarbonate and its application towards the reduction of 4-Nitrophenol. *Radiat. Phys. Chem.* **2019**, *162*, 126–130. [[CrossRef](#)]
17. Alwan, S.H.; Alshamsi, H.A. In situ synthesis NiO/F-MWCNTs nanocomposite for adsorption of malachite green dye from polluted water. *Carbon Lett.* **2022**. [[CrossRef](#)]
18. Mwafy, E.A.; Gaafar, M.S.; Mostafa, A.M.; Marzouk, S.Y.; Mahmoud, I.S. Novel laser-assisted method for synthesis of SnO₂/MWCNTs nanocomposite for water treatment from Cu (II). *Diam. Relat. Mater.* **2021**, *113*, 108287. [[CrossRef](#)]
19. Chen, H.; Zhao, J.; Zhong, A.; Jin, Y. Removal capacity and adsorption mechanism of heat-treated palygorskite clay for methylene blue. *Chem. Eng. J.* **2011**, *174*, 143–150. [[CrossRef](#)]
20. Taherian, Z.; Shahed Gharahshiran, V.; Khataee, A.; Meshkani, F.; Orooji, Y. Comparative study of modified Ni catalysts over mesoporous CaO–Al₂O₃ support for CO₂/methane reforming. *Catal. Commun.* **2020**, *145*, 106100. [[CrossRef](#)]
21. Faghhihinezhad, M.; Baghdadi, M.; Shahin, M.S.; Torabian, A. Catalytic ozonation of real textile wastewater by magnetic oxidized g-C₃N₄ modified with Al₂O₃ nanoparticles as a novel catalyst. *Sep. Purif. Technol.* **2022**, *283*, 120208. [[CrossRef](#)]
22. Gaudin, M.; Carles, P.; Laborde, E.; Champeaux, C.; Dumas-Bouchiat, F. A dual nanosecond-pulsed laser setup for nanocomposite synthesis—Ag nanoparticles in Al₂O₃/VO₂ matrix. *J. Appl. Phys.* **2019**, *125*, 054301. [[CrossRef](#)]
23. Fernandes, H.R.; Kapoor, S.; Patel, Y.; Ngai, K.; Levin, K.; Germanov, Y.; Krishtopa, L.; Kroeker, S.; Goel, A. Composition-structure-property relationships in Li₂O–Al₂O₃–B₂O₃ glasses. *J. Non-Cryst. Solids* **2018**, *502*, 142–151. [[CrossRef](#)]
24. Hu, H.; Saniger, J.; Castaño, V.M. Characterization of the mechanical properties of polyacrylic acid-metal oxide concretes. *Mater. Lett.* **1992**, *14*, 83–87. [[CrossRef](#)]
25. Trabelsi, A.B.G.; Alkallas, F.H.; Ziouche, A.; Boukhachem, A.; Ghamnia, M.; Elhouichet, H. Structural Defect Impact on Changing Optical Response and Raising Unpredicted Ferromagnetic Behaviour in (111) Preferentially Oriented Nanocrystalline NiO Films. *Crystals* **2022**, *12*, 692. [[CrossRef](#)]
26. Ding, S.; Fang, D.; Pang, Z.; Luo, B.; Kuang, L.; Wang, H.; Zhang, Q.; Shen, Q.; Ji, F. Immobilization of powdery calcium silicate hydrate via PVA covalent cross-linking process for phosphorus removal. *Sci. Total Environ.* **2018**, *645*, 937–945. [[CrossRef](#)]
27. Hassan, H.; Abidin, Z.H.Z.; Chowdhury, F.; Arof, A.K. A high efficiency chlorophyll sensitized solar cell with quasi solid PVA based electrolyte. *Int. J. Photoenergy* **2016**, *2016*, 3685210. [[CrossRef](#)]
28. Aslam, M.; Basit, M.; Ahmad, M.; Raza, Z.A. Structural and Band Structure Investigation of Iron Oxide Nanoparticles Incorporated PVA Nanocomposite Films. *Res. Sq.* **2021**. [[CrossRef](#)]
29. Mostafa, A.M.; Menazea, A.A. Polyvinyl Alcohol/Silver nanoparticles film prepared via pulsed laser ablation: An eco-friendly nano-catalyst for 4-nitrophenol degradation. *J. Mol. Struct.* **2020**, *1212*, 128125. [[CrossRef](#)]
30. Li, Y.; Lu, H.; Wang, Y.; Li, X. Deposition of Au nanoparticles on PDA-functionalized PVA beads as a recyclable catalyst for degradation of organic pollutants with NaBH₄ in aqueous solution. *J. Alloys Compd.* **2019**, *793*, 115–126. [[CrossRef](#)]
31. ElFaham, M.M.; Okil, M.; Mostafa, A.M. Fabrication of magnesium metallic nanoparticles by liquid-assisted laser ablation. *JOSA B* **2020**, *37*, 2620–2625. [[CrossRef](#)]
32. Mostafa, A.M.; Mwafy, E.A. The effect of laser fluence for enhancing the antibacterial activity of NiO nanoparticles by pulsed laser ablation in liquid media. *Environ. Nanotechnol. Monit. Manag.* **2020**, *14*, 100382. [[CrossRef](#)]
33. Mostafa, A.M.; Mwafy, E.A. Laser-assisted for preparation Ag/CdO nanocomposite thin film: Structural and optical study. *Opt. Mater.* **2020**, *107*, 110124. [[CrossRef](#)]
34. Mostafa, A.M.; Mwafy, E.A. Synthesis of ZnO/CdO thin film for catalytic degradation of 4-nitrophenol. *J. Mol. Struct.* **2020**, *1221*, 128872. [[CrossRef](#)]

35. Lam, J.; Lombard, J.; Dujardin, C.; Ledoux, G.; Merabia, S.; Amans, D.J.A.P.L. Dynamical study of bubble expansion following laser ablation in liquids. *Appl. Phys. Lett.* **2016**, *108*, 074104. [[CrossRef](#)]
36. Khan, S.Z.; Liu, Z.; Li, L. Characteristics of γ -Al₂O₃ nanoparticles generated by continuous-wave laser ablation in liquid. *Appl. Phys. A* **2010**, *101*, 781–787. [[CrossRef](#)]
37. Piriya Wong, V.; Thongpool, V.; Asanithi, P.; Limsuwan, P. Preparation and characterization of alumina nanoparticles in deionized water using laser ablation technique. *J. Nanomater.* **2012**, *2012*, 2. [[CrossRef](#)]
38. Riahi, A.; Khamlich, S.; Balghouthi, M.; Khamliche, T.; Doyle, T.B.; Dimassi, W.; Guizani, A.; Maaza, M. Study of thermal conductivity of synthesized Al₂O₃-water nanofluid by pulsed laser ablation in liquid. *J. Mol. Liq.* **2020**, *304*, 112694. [[CrossRef](#)]
39. Jafari Eskandari, M.; Shafeyi, A.; Karimzadeh, F. One-step fabrication of Au@Al₂O₃ core-shell nanoparticles by continuous-wave fiber laser ablation of thin gold layer on aluminum surface: Structural and optical properties. *Opt. Laser Technol.* **2020**, *126*, 106066. [[CrossRef](#)]
40. Menazea, A.A.; Mostafa, A.M.; Al-Ashkar, E.A. Effect of nanostructured metal oxides (CdO, Al₂O₃, Cu₂O) embedded in PVA via Nd:YAG pulsed laser ablation on their optical and structural properties. *J. Mol. Struct.* **2020**, *1203*, 127374. [[CrossRef](#)]
41. ElFaham, M.M.; Okil, M.; Mostafa, A.M. Effects of post-laser irradiation on the optical and structure properties of Al₂O₃ nanoparticles produced by laser ablation. *J. Appl. Phys.* **2020**, *128*, 153104. [[CrossRef](#)]
42. Li, X.; Hu, X.; Fu, Y.; Ai, H.; Fu, M.-L.; Yuan, B. Removal of phosphate at low concentration from water by porous PVA/Al₂O₃ composites. *Environ. Technol.* **2022**, *43*, 345–354. [[CrossRef](#)] [[PubMed](#)]
43. Rahman Khan, M.M.; Akter, M.; Amin, M.K.; Younus, M.; Chakraborty, N. Synthesis, Luminescence and Thermal Properties of PVA–ZnO–Al₂O₃ Composite Films: Towards Fabrication of Sunlight-Induced Catalyst for Organic Dye Removal. *J. Polym. Environ.* **2018**, *26*, 3371–3381. [[CrossRef](#)]
44. Karimi, Z.; Khalili, R.; Ali Zazouli, M. Surface modified polythiophene/Al₂O₃ and polyaniline/Al₂O₃ nanocomposites using poly (vinyl alcohol) for the removal of heavy metal ions from water: Kinetics, thermodynamic and isotherm studies. *Water Sci. Technol.* **2021**, *84*, 182–199. [[CrossRef](#)] [[PubMed](#)]
45. Mukwevho, N.; Gusain, R.; Fosso-Kankeu, E.; Kumar, N.; Waanders, F.; Ray, S.S. Removal of naphthalene from simulated wastewater through adsorption-photodegradation by ZnO/Ag/GO nanocomposite. *J. Ind. Eng. Chem.* **2020**, *81*, 393–404. [[CrossRef](#)]
46. Menazea, A.A.; Ezzat, H.A.; Omara, W.; Basyouni, O.H.; Ibrahim, S.A.; Mohamed, A.A.; Tawfik, W.; Ibrahim, M.A. Chitosan/graphene oxide composite as an effective removal of Ni, Cu, As, Cd and Pb from wastewater. *Comput. Theor. Chem.* **2020**, *1189*, 112980. [[CrossRef](#)]
47. Zulfiqar, M.; Lee, S.Y.; Mafize, A.A.; Kahar, N.A.M.A.; Johari, K.; Rabat, N.E. Efficient Removal of Pb(II) from Aqueous Solutions by Using Oil Palm Bio-Waste/MWCNTs Reinforced PVA Hydrogel Composites: Kinetic, Isotherm and Thermodynamic Modeling. *Polymers* **2020**, *12*, 430. [[CrossRef](#)]
48. Inagaki, M.; Fujita, K.; Takeuchi, Y.; Oshida, K.; Iwata, H.; Konno, H. Formation of graphite crystals at 1000–1200 °C from mixtures of vinyl polymers with metal oxides. *Carbon* **2001**, *39*, 921–929. [[CrossRef](#)]
49. Shojaei, B.; Miri, R.; Bazyari, A.; Thompson, L.T. Asphaltene adsorption on MgO, CaO, SiO₂, and Al₂O₃ nanoparticles synthesized via the Pechini-type Sol–Gel method. *Fuel* **2022**, *321*, 124136. [[CrossRef](#)]
50. Hema, M.; Selvasekarapandian, S.; Arunkumar, D.; Sakunthala, A.; Nithya, H.F.T.I.R. FTIR, XRD and ac impedance spectroscopic study on PVA based polymer electrolyte doped with NH₄X (X = Cl, Br, I). *J. Non-Cryst. Solids* **2009**, *355*, 84–90. [[CrossRef](#)]
51. Darwish, A.M.; Eisa, W.H.; Shabaka, A.A.; Talaat, M.H. Synthesis of nano-cadmium sulfide by pulsed laser ablation in liquid environment. *Spectrosc. Lett.* **2015**, *48*, 638–645. [[CrossRef](#)]
52. Milanović, P.; Vuksanović, M.M.; Mitrić, M.; Stojanović, D.B.; Kojović, A.; Rogan, J.R.; Jančić-Heinemann, R. Electrospun alumina fibers doped with ferric and magnesium oxides. *Sci. Sinter.* **2018**, *50*, 77–83. [[CrossRef](#)]
53. Singh, D.; Gautam, R.K.; Kumar, R.; Shukla, B.K.; Shankar, V.; Krishna, V. Citric acid coated magnetic nanoparticles: Synthesis, characterization and application in removal of Cd(II) ions from aqueous solution. *J. Water Process Eng.* **2014**, *4*, 233–241. [[CrossRef](#)]
54. Zhou, Q.; Wang, X.; Liu, J.; Zhang, L. Phosphorus removal from wastewater using nano-particulates of hydrated ferric oxide doped activated carbon fiber prepared by Sol–Gel method. *Chem. Eng. J.* **2012**, *200–202*, 619–626. [[CrossRef](#)]
55. Singh, D.K.; Mishra, S. Synthesis, characterization and removal of Cd(II) using Cd(II)-ion imprinted polymer. *J. Hazard. Mater.* **2009**, *164*, 1547–1551. [[CrossRef](#)] [[PubMed](#)]
56. Chaudhry, A.N.; Billingham, N.C. Characterisation and oxidative degradation of a room-temperature vulcanised poly(dimethylsiloxane) rubber. *Polym. Degrad. Stab.* **2001**, *73*, 505–510. [[CrossRef](#)]
57. Mwafy, E.A.; Mostafa, A.M. Efficient removal of Cu (II) by SnO₂/MWCNTs nanocomposite by pulsed laser ablation method. *Nano-Struct. Nano-Objects* **2020**, *24*, 100591. [[CrossRef](#)]
58. Xie, J.; Lin, Y.; Li, C.; Wu, D.; Kong, H. Removal and recovery of phosphate from water by activated aluminum oxide and lanthanum oxide. *Powder Technol.* **2015**, *269*, 351–357. [[CrossRef](#)]
59. Hasan, Z.; Jhung, S.H. Removal of hazardous organics from water using metal-organic frameworks (MOFs): Plausible mechanisms for selective adsorptions. *J. Hazard. Mater.* **2015**, *283*, 329–339. [[CrossRef](#)]
60. Dias, E.M.; Petit, C. Towards the use of metal–organic frameworks for water reuse: A review of the recent advances in the field of organic pollutants removal and degradation and the next steps in the field. *J. Mater. Chem. A* **2015**, *3*, 22484–22506. [[CrossRef](#)]

61. Acelas, N.Y.; Martin, B.D.; López, D.; Jefferson, B. Selective removal of phosphate from wastewater using hydrated metal oxides dispersed within anionic exchange media. *Chemosphere* **2015**, *119*, 1353–1360. [[CrossRef](#)] [[PubMed](#)]
62. Dubey, S.; Banerjee, S.; Upadhyay, S.N.; Sharma, Y.C. Application of common nano-materials for removal of selected metallic species from water and wastewaters: A critical review. *J. Mol. Liq.* **2017**, *240*, 656–677. [[CrossRef](#)]
63. Yi, R.; Guo, L.; Zou, X.; Li, J.; Hao, Z.; Yang, X.; Li, X.; Zeng, X.; Lu, Y.F. Background removal in soil analysis using laser-induced breakdown spectroscopy combined with standard addition method. *Opt. Express* **2016**, *24*, 2607–2618. [[CrossRef](#)]
64. Guo, P.; Tang, L.; Tang, J.; Zeng, G.; Huang, B.; Dong, H.; Zhang, Y.; Zhou, Y.; Deng, Y.; Ma, L. Catalytic reduction–adsorption for removal of p-nitrophenol and its conversion p-aminophenol from water by gold nanoparticles supported on oxidized mesoporous carbon. *J. Colloid Interface Sci.* **2016**, *469*, 78–85. [[CrossRef](#)]
65. Gao, Q.; Xu, J.; Bu, X.-H. Recent advances about metal–organic frameworks in the removal of pollutants from wastewater. *Coord. Chem. Rev.* **2019**, *378*, 17–31. [[CrossRef](#)]
66. Arizavi, A.; Mirbagheri, N.S.; Hosseini, Z.; Chen, P.; Sabbaghi, S. Efficient removal of naphthalene from aqueous solutions using a nanoporous kaolin/Fe₃O₄ composite. *Int. J. Environ. Sci. Technol.* **2020**, *17*, 1991–2002. [[CrossRef](#)]
67. Abbas, S.; Nasreen, S.; Haroon, A.; Ashraf, M.A. Synthesis of Silver and Copper Nanoparticles from Plants and Application as Adsorbents for Naphthalene decontamination. *Saudi J. Biol. Sci.* **2020**, *27*, 1016–1023. [[CrossRef](#)]
68. Gao, R.; Fu, Q.; Hu, H.; Wang, Q.; Liu, Y.; Zhu, J. Highly-effective removal of Pb by co-pyrolysis biochar derived from rape straw and orthophosphate. *J. Hazard. Mater.* **2019**, *371*, 191–197. [[CrossRef](#)]